Theoretical Investigation on Electronic Structure and Photophysical Properties of a Series of Mixed-Carbene Cyclometalated Iridium(III) Complexes With Different Ancillary Ligand Applied in Phosphorescent Organic Light-Emitting Diodes

Tong Chen
College of Chemistry and Life Science, Changchun University of Technology
Deming Han
School of Life Science and Technology, Changchun University of Science and Technology
Lihui Zhao
School of Life Science and Technology, Changchun University of Science and Technology
Bao Wang
College of Chemistry and Life Science, Changchun University of Technology
Xiaohong Shang (shangxiaohong58@aliyun.com)
College of Chemistry and Life Science, Changchun University of Technology

Research Article

Keywords: DFT , TDDFT , OLEDs , Iridium , Phosphorescence

Posted Date: April 26th, 2021

DOI: https://doi.org/10.21203/rs.3.rs-410004/v1

Version of Record: A version of this preprint was published at Journal of Computational Electronics on July 13th, 2021. See the published version at https://doi.org/10.1007/s10825-021-01738-z.

Theoretical investigation on electronic structure and photophysical properties of a series of mixed-carbene cyclometalated iridium(III) complexes with different ancillary ligand applied in phosphorescent organic light-emitting diodes

Tong Chen[1] · Deming Han[2,3] · Lihui Zhao[2] · Bao Wang[1] · Xiaohong Shang[1]

Abstract

By using density functional theory (DFT) and time-dependent density functional theory (TDDFT), the geometrical structure, electronic structure and photophysical properties of a series of mixed-carbene cyclometalated iridium(III) complexes with different ancillary ligand have been explored. The frontier molecular orbital (FMO) components and energy levels for all studied complexes have been investigated. The lowest lying absorptions were calculated to be at 327, 322, 333, 332 and 332 nm for these complexes, which have the transition configuration of HOMO→LUMO. The lowest energy emissions for these complexes are localized at 413, 399, 498, 418 and 415 nm, respectively, simulated in CH_2Cl_2 medium at the M062X level. One complex designed could possess the largest radiative decay rate (k_r) value and be a potential candidate for blue emitters in organic light-emitting diodes (OLEDs). The theoretical study can provide a useful guidance for design and synthesis of new iridium(III) complexes in phosphorescent materials.

Keywords DFT · TDDFT · OLEDs · Iridium · Phosphorescence

✉ Xiaohong Shang and Deming Han

shangxiaohong58@aliyun.com (X. Shang) and handeming2009@yahoo.com (D. Han).

[1] College of Chemistry and Life Science, Changchun University of Technology, Changchun 130012, P. R. China

[2] School of Life Science and Technology, Changchun University of Science and Technology, Changchun 130022, P. R. China

[3] Jilin Provincial Science and Technology Innovation Center of Optical Materials and Chemistry, Changchun, 130022, P. R. China

1 Introduction

In recent two decades, organic light-emitting diodes (OLEDs) have been widely studied due to their applications in flat display and light sources [1–5]. Phosphorescent OLEDs can capture singlet excitons and triplet excitons at the same time due to the heavy atom effect, so theoretically 100% internal quantum yield can be achieved. Among them, phosphorescent iridium complexes have received the most attention [6–10]. Recently, the phosphorescence color and quantum efficiency have been widely investigated by theoretical and experimental researchers. Many green and red-emitting OLEDs devices with excellent performances have been reported. However, the development of blue-emitting phosphors still remains a challenging task to achieve high efficiency and stability for blue phosphorescence [11–13]. In order to obtain full-color display, it is necessary to obtain commercially available red, green, and blue light materials. Among them, the blue emitters require a wide energy gap between the excited triplet state and the ground state. The approaches to obtain efficient phosphorescent blue emitting materials are to either seek ligands with high triplet energy or use electron-withdrawing ancillary ligands to raise the emission energy by stabilizing/destabilizing the highest occupied/lowest unoccupied molecular orbital (HOMO/LUMO).

N-heterocyclic carbenes (NHCs) are typical carbene ligands incorporated into blue-emitting iridium complexes [14–16]. The acyclic diaminocarbenes (ADCs) can be even stronger σ-donors than NHCs on account of the greater 2p character in their σ orbital [17,18], which could potentially destabilize metal-centered triplet excited state (^{3}MC) to an even greater extent than is possible with NHCs and improve the photostability of blue phosphorescent complexes. Recently, Hanah Na *et al.* have investigated a class of cyclometalated iridium complexes with general structure Ir(C^C:^{NHC})$_2$(C^C:^{ADC}), where C^C:^{NHC} is an N-heterocyclic carbene (NHC) derived cyclometalating ligand and C^C:^{ADC} is a different type of cyclometalating ligand featuring an acyclic diaminocarbene (ADC) [19]. In this study, on the basis of complex 3b [19], that is, complex **1** in Fig. 1, four complexes [**2**, **3**, **4** and **5** in Fig. 1(a)] have been designed. The electronic structures and photophysical properties of these complexes have been theoretically studied by using density functional theory (DFT) and time-dependent density functional theory (TDDFT). The ancillary ligand with different substituent group will have an effect on the electronic structure and photophysical properties of all the studied complexes.

2 Computational methods

To calculate electronic singlet and triplet states of all the studied complexes, we use the DFT (density functional theory) with PBE0 (hybrid-type Perdew–Burke–Ernzerhof exchange correlation functional) and UPBE0 (unrestricted PBE0) respectively [20–22]. The value of lowest-lying emission wavelength of complex **1** is calculated by M062X method which is in good agreement with the experimental wavelength value [19]. The quasi-relativistic pseudopotentials of Ir atom proposed by Hay and Wadt with 17 valence electrons were employed, and a ‘‘double-ξ’’ quality basis set LANL2DZ was adopted as the basis set [23]. The 6–31G(d) basis set was employed to other atoms. Based on the optimized structures of the ground and excited states, the time-dependent DFT (TDDFT) approach associated with the SCRF (self-consistent reaction field) theory using the integral equation formalism polarized continuum model (IEFPCM) [24–26] in dichloromethane (CH_2Cl_2) media was applied to simulate the absorption and emission spectral properties from the experimental results by Hanah Na *et al*. [19]. All calculations were performed by using the Gaussian 09 software package [27]. GaussSum 2.5 is used for UV/Vis absorption spectra analysis with a full width at half maximum (FWHM) of 3000 cm^{-1} based on the present TDDFT computational results [28].

3 Results and discussion

3.1 Geometries in the ground state S_0 and triplet excited state T_1

The sketch map of Ir(III) complexes **1**–**5** has been presented in Fig. 1(a), and the partial atomic number of complex **1** as a representative has been shown in Fig. 1(b). In order to describe these complexes, the main ligand and ancillary ligand have been respectively named as NHC and ADC moieties. The main optimized geometry parameters of the ground state S_0 and triplet excited state T_1 are presented in Table 1.

The optimized bond distances of complex **1** are in quite good agreement with available experimental data [19], and the deviation is within 1.8%. The bond angles C1–Ir–C2, C3–Ir–C6 and C4–Ir–C5 are larger than 77°. The bond angles C1–Ir–C6, C2–Ir–C5 and C3–Ir–C4 are larger than 166°. This indicates that all studied Ir(III) complexes with d^6 configuration adopt a pseudo-octahedral coordination geometry. The dihedral angles

C1–C3–C6–C4 in complexes **1**–**5** are less than 2°, which shows a nearly plane structure around the central Ir atom. Especially, the dihedral angle C1–C2–C6–C5 in complex **2** is less than those of other four complexes, which is probably due to the introduction of the strong electron-donating group —$N(CH_3)_2$. From the S_0 to T_1 states, the bond lengths Ir–C4 and Ir–C5 in complexes **1**–**5** slightly decrease and increase, respectively. The bond angles C3–Ir–C6 and C4–Ir–C5 in complexes **1**–**5** also slightly decrease and increase, respectively.

3.2 Frontier molecular orbitals (FMOs) properties

The frontier molecular orbital (FMO) properties are bound up with the photophysical properties of these Ir(III) complexes. The energy levels and distributions of the highest occupied molecular orbital (HOMO) and lowest unoccupied molecular orbital (LUMO) of all studied Ir(III) complexes have been investigated by DFT/PBE0 method. The contour plots of HOMO and LUMO are shown in Fig. 2. The detailed descriptions of the molecular orbitals, in terms of energies, composition and the assignment of different fragments have been collected in Tables S1–S5 (Supplementary Information). From Fig. 2 and Tables S1–S5, it can be seen that the HOMO of complexes **1**–**4** resides mainly on the Ir atom and NHC ligand. For example, the HOMO of **1** distributes over the d-orbital of Ir (36%) and the π-orbital of NHC (58%). However, the HOMO of complex **5** distributes on the Ir atom (31%), NHC (40%) and ADC (29%) ligand. The LUMO of all studied complexes resides mainly on the NHC ligand except complex **3**, which mainly distributes on ADC ligand. Besides, the HOMO/LUMO energy levels for complexes **1**–**5** are not largely different. The largest and smallest energy gaps between LUMO and HOMO ($\Delta E_{L\rightarrow H}$) values are 4.76 and 4.61 eV for complexes **2** and **5**, respectively.

3.3 Absorption spectra

The vertical electronic excitation energies, oscillator strengths (f), dominant orbital excitations and their assignments of the singlet excited state are presented in Table S6 (Supplementary Information). Simulated absorption curves for complexes **1**–**5** in CH_2Cl_2 medium have been depicted in Fig. 3.

The absorption spectra shapes of complexes **1**–**5** are very similar. In addition, there is a small absorption peak at about 260 nm for complexes **4** and **5**. It can be seen from Table S6 that the lowest lying singlet→singlet absorption of **1**–**5** is located at 327 nm (f = 0.0103), 322

nm (f = 0.0038), 333 nm (f = 0.0023), 332 nm (f = 0.0092) and 332 nm (f = 0.0077), respectively. The calculated 327 nm absorption for complex **1** can be comparable to the experimental value of 302 nm [19]. The lowest lying absorptions for complexes **1**, **2** and **4** mainly have the HOMO→LUMO transition configuration contributing to the $S_0 \rightarrow S_1$ state, and they have the same transitions; for example, the lowest energy absorption of **1** is characterized as metal-to-ligand charge transfer (MLCT)/intraligand charge transfer (ILCT) [d(Ir)+π(NHC)→π*(NHC)] character. The lowest lying absorptions for complex **3** have the HOMO→LUMO transition configuration contributing to the $S_0 \rightarrow S_1$ state characterized as MLCT/ligand-to-ligand charge transfer (LLCT) d(Ir)+π(NHC)→π*(ADC) character. For complex **5**, the lowest energy absorption is characterized as MLCT/LLCT/ILCT [d(Ir)+π(NHC+ADC)→π*(NHC)].

3.4 Phosphorescence emission properties

In order to further explore the phosphorescent properties of the complexes, the TDDFT method was used to calculate the emission wavelength and transition properties based on the optimized T_1 structure. In order to ensure the accuracy of the data, the density functionals B3LYP [29], PBE0 [30], CAM-B3LYP [31], M052X [32], M062X [33] and BP86 [34] were respectively used to calculate the complex **1**. The calculated lowest energy emissions at these levels are localized at 2.356, 2.467, 2.808, 3.013, 3.001 and 1.908 eV, deviating from experimental value 2.952 eV [19] by 0.596, 0.485, 0.144, 0.061, 0.049 and 1.051 eV. Obviously, a good agreement with measured datum was obtained for M062X. Therefore, we have employed the M062X method for emission property calculations of all studied complexes. The calculated emission wavelengths, emission energies and transition nature of complexes **1**–**5** in CH_2Cl_2 medium at the M062X level are listed in Table 2. The plots of the molecular orbitals related to emissions of complexes **1**–**5** have also been presented in Table 3. In addition, partial frontier molecular orbital compositions (%) of complexes **1**–**5** in the triplet excited states are presented in Table S7 (Supplementary Information).

Table 2 shows that the calculated lowest energy emissions of complexes **1**–**5** are located at 413, 399, 498, 418 and 415 nm, respectively. Complex **3** has the largest emission wavelength 498 nm among these studied complexes, which shows the introduction of phenyl ring to the ancillary ligand has an obvious effect on the phosphorescence emission properties. From Table 2 and Table S7, it can be seen that the phosphorescence emission of all studied

complexes mainly possesses the transition of LUMO→HOMO configuration. For example, complex **1** has the triplet metal-to-ligand charge transfer (^{3}MLCT)/triplet ligand-to-ligand charge transfer (^{3}LLCT)/triplet intraligand charge transfer (^{3}ILCT) [π*(NHC)→d*(Ir)+π*(NHC+ADC)] transition characters. Complex **2** has the smallest emission wavelength 399 nm among these studied complexes, which may be due to the introduction of —$N(CH_3)_2$ with strong electron-donating ability to the ancillary ligand. For example, the LUMO of complex **1** is distributed on the NHC ligand (91%). From Table 3 and Table S7, it can be seen that the LUMO of all studied complexes are mainly localized on the NHC ligand except complex **3**. The HOMO of all studied complexes are mainly localized on the Ir atom and NHC ligand. For example, the HOMO of complex **1** is distributed on Ir atom (34%) and NHC ligand (55%).

3.5 Phosphorescence quantum yield

The phosphorescent quantum yield (Φ_{PL}) is obtained by the following equation [35]:

$$\Phi_{PL} = \frac{k_r}{k_r + k_{nr}} \qquad (1)$$

in which k_r is the radiative decay rate and k_{nr} is the nonradiative decay rate. Therefore, it is necessary to increase k_r and reduce k_{nr} to achieve high phosphorescent quantum efficiency. The k_{nr} from the T_1 to the S_0 states is usually expressed in the form of the energy law equation (2), and the k_r is given by equation (3) [36,37]:

$$k_{nr} \propto \alpha \exp(-\beta E_{T_1}) \qquad (2)$$

$$k_r \approx \gamma \frac{\left\langle \psi_{S_1} \middle| H_{S_0} \middle| \psi_{T_1} \right\rangle^2 \mu_{S_1}^2}{(\Delta E_{S_1\text{-}T_1})^2} \qquad (3)$$

$$\gamma = 16\pi^3 10^6 n^3 E_{em}{}^3 / 3h\varepsilon_0$$

Here, α, β and γ are constant, μ_{s_1} is the transition electric dipole moment for the $S_0 \rightarrow S_1$ transition, E_{T_1} represents the emission energy in cm^{-1}, and n, h, and ε_0 are the refractive index of the medium, Planck's constant, and the permittivity in vacuo, respectively. $\left\langle \Psi_{S_1} \middle| H_{S_0} \middle| \Psi_{T_1} \right\rangle$ is the spin–orbit couplings (SOC) matrix element. In addition, the SOC

effects can be elucidated by the triplet metal-to-ligand charge transfer (^{3}MLCT) in the T_1 state [38]. It is known that a larger ^{3}MLCT composition and thus the intersystem crossing (ISC) can increase the phosphorescence quantum yield. The direct involvement of the d(Ir) orbital can increase the first-order SOC in the $T_1 \rightarrow S_0$ transition, resulting in a drastic decrease of the radiative lifetime and an increased nonradiative rate constant. The ^{3}MLCT contribution of complex **4** is the largest one among these studied complexes. The phosphorescence quantum yield is inversely proportional to the energy gaps between the S_1 and T_1 states ($\Delta E_{S_1-T_1}$) [39], which a minimal $\Delta E_{S_1-T_1}$ is required for enhancing the intersystem crossing rate, leading to the increased k_r. The $\Delta E_{S_1-T_1}$ and μ_{s_1} values have been presented in Table 4. As mentioned above, according to equation (1), a lower $\Delta E_{S_1-T_1}$ and larger ^{3}MLCT contributions and higher μ_{s_1} values may account for a larger k_r. Hence, the complex **4** possibly possesses the largest k_r value, which might be a potential candidate for blue emitters in phosphorescent dopant emitters in OLEDs.

4 Conclusions

In this study the electronic structures and photophysical properties of five iridium(III) complexes with different ancillary ligand have been theoretically investigated. All studied complexes have a distorted octahedral structures around the Ir(III) metal center with d^6 configuration. The HOMO/LUMO energy levels for complexes **1**–**5** in the S_0 state are not largely changed. Complexes **1**–**5** have the similar absorption curves with a large peak. The calculated phosphorescent emission wavelength of complex **1** at TDDFT/M062X level shows a very good agreement with the available experimental datum. The HOMO of complexes **1**–**5** in the T_1 state are mainly localized on the Ir atom and NHC ligand. Complex **4** has the largest ^{3}MLCT contribution among these studied complexes. It is anticipated that this study will be good for the further theoretical and experimental design of phosphorescent materials in OLEDs.

Acknowledgements The authors are grateful to the financial aid from the Program of Science and Technology Development Plan of Jilin Province of China (Grant No. 20200201099JC). The authors are grateful to Computing Center of Jilin Province of China and Professor Keli Han of Dalian Institute of Chemical Physics, Chinese Academy of Sciences for essential support.

Compliance with ethical standards

Conflict of interest The authors declare that they have no conflicts of interest.

References

1. Bullock, J.D., Xu, Z.T., Valandro, S., Younus, M., Xue, J.G., Schanze, K.S., ACS Appl. Electron. Mater. **2**, 1026–1034 (2020)
2. Yang, Z., Mao, Z., Xu, C., Chen, X.J., Zhao, J., Yang, Z.Y., Zhang, Y., Wu, W., Jiao, S.B., Liu, Y., Aldred, M.P., Chi, Z.G., Chem. Sci. **10**, 8129–8134 (2019)
3. Woo, Y., Hong, W., Yang, S.Y., Kim, H.J., Cha, J.H., Lee, J.E., Lee, K.J., Kang, T., Choi, S.Y., Adv. Electron. Mater. **4**, 1800251 (2018)
4. Zhang, T.Z., Shi, C.S., Zhao, C.Y., Wu, Z.B., Sun, N., Chen, J.S., Xie, Z.Y., Ma, D.G., J. Mater. Chem. C **5**, 12833–12838 (2017)
5. Sharma, R.K., Deepak, Katiyar, M., Org. Electron. **38**, 121–129 (2016)
6. Ding, Y., Liu, D., Li, J.Y., Li, H.T., Ma, H.Y., Li, D.L., Niu, R., Dyes Pigm. **179**, 108405 (2020)
7. Hsu, L.Y., Liang, Q.M., Wang, Z.H., Kuo, H.H., Tai, W.S., Su, S.J., Zhou, X.W., Yuan, Y., Chi, Y., Chem. Eur. J. **25**, 15375–15386 (2019)
8. Wang, Y., Bao, P., Wang, J., Jia, R., Jia, R., Bai, F.Q., Zhang, H.X., Inorg. Chem. **57**, 6561–6570 (2018)
9. Wang, Y., Bai, F.Q., Ma, X.Y., Zhang, H.X., Org. Electron. **59**, 293–300 (2018)
10. Mi, B.X., Zhong, C., Sang, J., Liao, Z.J., Wang, H.J., Gao, Z.Q., J. Lumin. **180**, 51–57 (2016)
11. Yang, X., Xu, X., Zhou, G., J. Mater. Chem. C **3**, 913–944 (2015)
12. Visbal, R., Gimeno, M.C., Chem. Soc. Rev. **43**, 3551–3574 (2014)
13. Chou, P.T., Chi, Y., Chung, M.W., Lin, C.C., Coord. Chem. Rev. **255**, 2653–2665 (2011)
14. Pal, A.K., Krotkus, S., Fontani, M., Mackenzie, C.F.R., Cordes, D.B., Slawin, A.M.Z., Samuel, I.D.W., Zysman-Colman, E., Adv. Mater. **30**, 1804231 (2018)
15. Chen, Z., Wang, L., Su, S., Zheng, X., Zhu, N., Ho, C.L., Chen, S., Wong, W.Y., ACS Appl. Mater. Interfaces **9**, 40497–40502 (2017)
16. Lee, J., Chen, H.F., Batagoda, T., Coburn, C., Djurovich, P.I., Thompson, M.E., Forrest, S.R., Nat. Mater. **15**, 92–98 (2015)

17. de Frémont P., Marion, N., Nolan, S.P., Coord. Chem. Rev. **253**, 862–892 (2009)
18. Boyarskiy, V.P., Luzyanin, K.V., Yu. Kukushkin, V., Coord. Chem. Rev. **256**, 2029–2056 (2012)
19. Na, H., Cañada, L.M., Wen, Z.L., Wu, J.C., Teets, T.S., Chem. Sci. **10**, 6254 (2019)
20. Burke, K., Werschnik, J., Gross, E.K.U., J. Chem. Phys. **123**, 062206 (2005)
21. Perdew, J.P., Burke, K., Ernzerhof, M., Phys. Rev. Lett. **77**, 3865–3868 (1996)
22. Perdew, J.P., Burke, K., Ernzerhof, M., Phys. Rev. Lett. **80**, 891 (1998)
23. Hay, P.J., Wadt, W.R., J. Chem. Phys. **82**, 270–283 (1985)
24. Stratmann, R.E., Scuseria, G.E., Frisch, M.J., J. Chem. Phys. **109**, 8218–8224 (1998)
25. Cossi, M., Barone, V., Mennucci, B., Tomasi, J., Chem. Phys. Lett. **286**, 253–260 (1998)
26. Mennucci, B., Tomasi, J., J. Chem. Phys. **106**, 5151–5155 (1997)
27. Frisch, M.J., Trucks, G.W., Schlegel, H.B., Scuseria, G.E., Robb, M.A., Cheeseman, J.R., Scalmani, G., Barone, V., Mennucci, B., Petersson, G.A., Nakatsuji, H., Caricato, M., Li, X., Hratchian, H.P., Izmaylov, A.F., Bloino, J., Zheng, G., Sonnenberg, J.L., Hada, M., Ehara, M., Toyota, K., Fukuda, R., Hasegawa, J., Ishida, M., Nakajima, T., Honda, Y., Kitao, O., Nakai, H., Vreven, T., Montgomery, J.A. Jr., Peralta, J.E., Ogliaro, F., Bearpark, M., Heyd, J.J., Brothers, E., Kudin, K.N., Staroverov, V.N., Kobayashi, R., Normand, J., Raghavachari, K., Rendell, A., Burant, J.C., Iyengar, S.S., Tomasi, J., Cossi, M., Rega, N., Millam, N. J., Klene, M., Knox, J.E., Cross, J.B., Bakken, V., Adamo, C., Jaramillo, J., Gomperts, R., Stratmann, R.E., Yazyev, O., Austin, A.J., Cammi, R., Pomelli, C., Ochterski, J.W., Martin, R.L., Morokuma, K., Zakrzewski, V.G., Voth, G.A., Salvador, P., Dannenberg, J.J., Dapprich, S., Daniels, A.D., Farkas, ö., Foresman, J.B., Ortiz, J.V., Cioslowski, J., Fox, D.J., Gaussian 09; Gaussian, Inc.; Wallingford, CT, 2009.
28. O'Boyle, N.M., Tenderholt, A.L., Langner, K.M., J. Comput. Chem. **29**, 839–845 (2008)
29. Niehaus, T.A., Hofbeck, T., Yersin, H., RSC Adv. **5**, 63318–63325 (2015)
30. Perdew, J.P., Burke, K., Ernzerhof, M., Phys. Rev. Lett. **77**, 3865–3868 (1996)
31. Cramer, C., Truhlar, D., Solvent Effects and Chemical Reactivity, Kluwer, Dordrecht, The Netherlands, (1996)
32. Zhao, Y., Schultz, N.E., Truhlar, D.G., J. Chem. Theory Comput. **2**, 364–382 (2006)
33. Zhao, Y., Truhlar, D.G., Theor. Chem. Acc. **120**, 215–241 (2008)
34. Perdew, J.P., Phys. Rev. B: Condens. Matter Mater. Phys. **33**, 8822–8824 (1986)

35. Ito, A., Meyer, T.J., Phys. Chem. Chem. Phys. **14**, 13731–13745 (2012)
36. Haneder, S., Como, E.D., Feldmann, J., Lupton, J.M., Lennartz, C., Erk, P., Fuchs, E., Molt, O., Münster, I., Schildknecht, C., Wagenblast, G., Adv. Mater. **20**, 3325–3330 (2008)
37. Minaev, B., Baryshnikov, G., Agren, H., Phys. Chem. Chem. Phys. **16**, 1719–1758 (2014)
38. Chai, J.D., Head-Gordon, M., Phys. Chem. Chem. Phys. **10**, 6615–6620 (2008)
39. Avilov, I., Minoofar, P., Cornil, J., De Cola, L., J. Am. Chem. Soc. **129**, 8247–8258 (2007)

Figures and Tables:

(a)

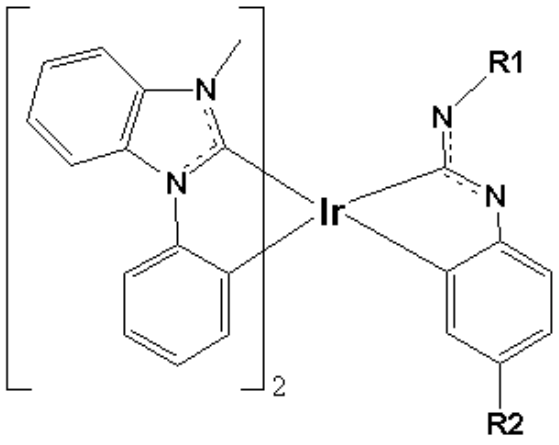

1: R1 = Propyl R2 = -CF_3

2: R1 = CH_3 / CH_3 R2 = -CF_3

3: R1 = Ph R2 = -CF_3

4: R1 = Propyl R2 = -H

5: R1 = Propyl R2 = -OCH_3

(b)

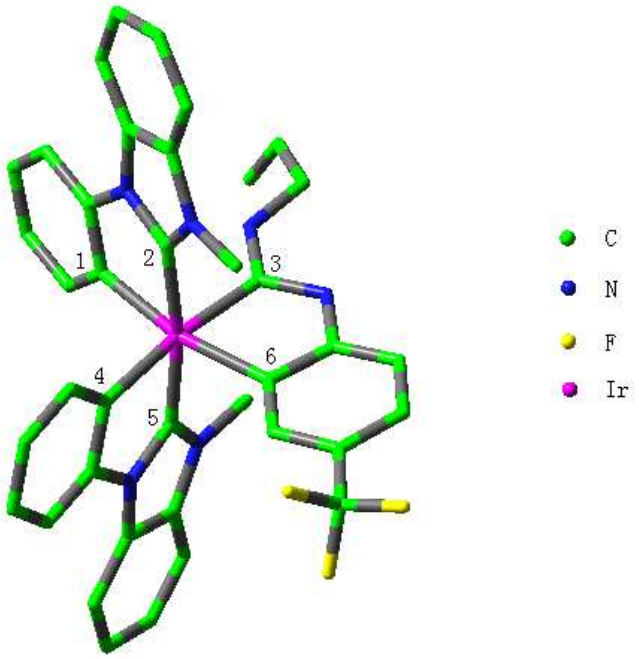

Fig. 1 (a) Sketch map of the structures of Ir(III) complexes **1–5**. (b) Representative optimized structure of **1** in the ground state at the PBE0 level (H atoms omitted).

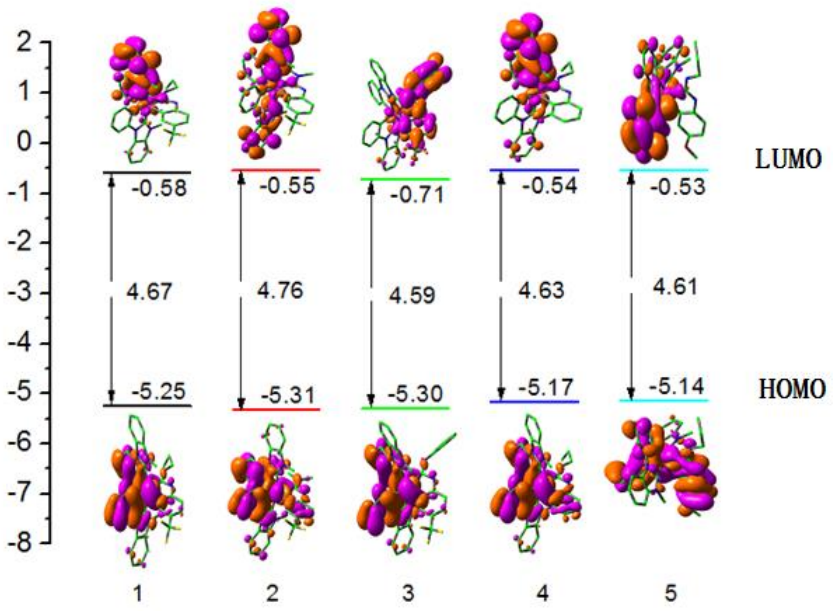

Fig. 2 Contour plots of the HOMO and LUMO for complexes **1**–**5** in S_0 state. The unit of data is eV.

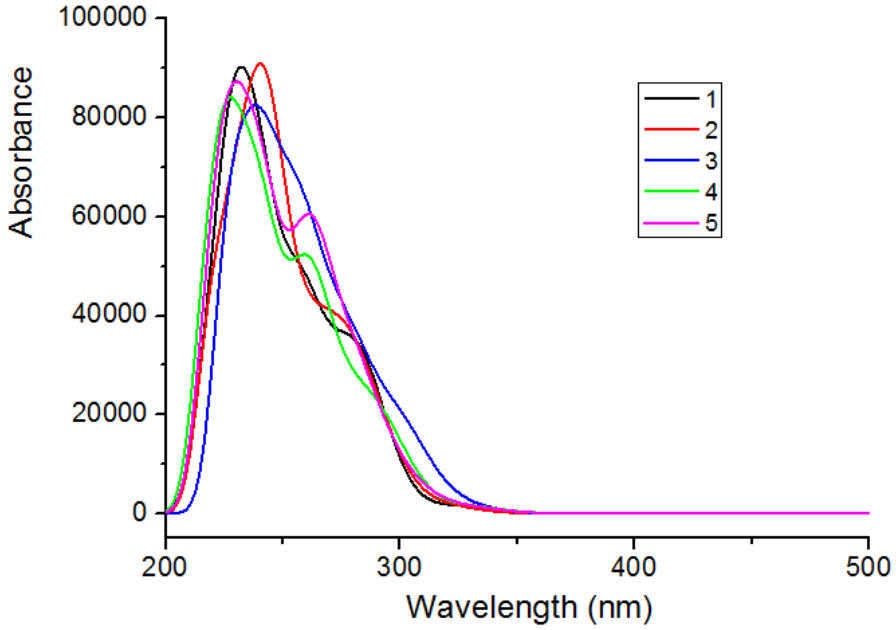

Fig. 3 Simulated absorption spectra of complexes **1**–**5** in CH_2Cl_2 media.

Table 1 Main optimized geometry parameters of complexes **1**–**5** in the ground and the lowest

lying triplet states, together with the experimental values

	1		**2**		**3**		**4**		**5**	
	S_0	T_1	S_0	T_1	S_0	T_1	S_0	T_1	S_0	T_1
	PBE0/Exptl.[a]									
bond length (Å)										
Ir–C1	2.085/2.096	2.058	2.094	2.101	2.085	2.053	2.086	2.067	2.086	2.061
Ir–C2	2.034/2.026	2.105	2.032	2.030	2.034	2.037	2.032	2.098	2.032	2.099
Ir–C3	2.055/2.019	2.102	2.114	2.129	2.050	2.151	2.057	2.111	2.058	2.110
Ir–C4	2.074/2.081	2.028	2.063	2.019	2.077	2.035	2.075	2.030	2.073	2.030
Ir–C5	2.018/1.997	2.028	2.021	2.034	2.021	2.028	2.018	2.026	2.018	2.029
Ir–C6	2.101/2.094	2.106	2.099	2.100	2.100	2.129	2.106	2.102	2.106	2.106
bond angle (deg)										
C1–Ir–C2	78.04/77.81	79.36	77.96	77.94	77.97	79.15	78.00	79.35	78.03	79.39
C3–Ir–C6	78.61/79.57	76.71	78.72	78.46	78.57	76.71	78.64	76.62	78.73	76.70
C4–Ir–C5	78.11/77.70	78.76	78.30	79.62	77.95	79.04	78.05	78.58	78.04	78.67
C1–Ir–C6	170.71/168.19	162.63	177.17	177.64	171.25	160.74	170.41	161.48	170.45	161.95
C2–Ir–C5	166.82/170.67	170.93	167.79	168.79	166.73	174.03	167.40	170.38	167.55	170.83
C3–Ir–C4	172.75/171.99	169.43	169.72	168.58	171.98	166.21	172.43	171.05	172.47	170.51
dihedral angle (deg)										
C1–C2–C6–C5	14.36/12.19	17.59	3.74	3.02	13.97	16.92	14.30	18.56	14.15	18.27
C2–C3–C5–C4	10.49/11.18	11.88	13.09	13.85	11.28	14.05	10.50	11.03	10.43	11.02
C1–C3–C6–C4	0.77/4.19	3.29	0.59	0.51	0.03	1.28	1.09	4.85	1.27	3.45

[a] Ref. 19

Table 2 The calculated emission wavelength (nm) in CH_2Cl_2 medium at the TDDFT/M062X level for complexes **1**–**5**, along with the major contribution and transition characters

	λ(nm)/E(eV)	Configuration	Nature	Exptl.[a]
1	413/ 3.00	L→H (79%)	MLCT/LLCT/ILCT	420 nm
2	399/ 3.10	L→H (62%)	MLCT/ILCT	
3	498/ 2.48	L→H (70%)	MLCT/LLCT	
4	418/ 2.95	L→H (80%)	MLCT/LLCT/ILCT	
5	415/ 2.98	L→H (79%)	MLCT/LLCT/ILCT	

[a] Ref. 19

Table 3 Contour plots of the HOMO and LUMO for complexes **1**–**5** in T_1 state, which are transitions responsible for the emissions at 413, 399, 498, 418 and 415 nm for complexes **1**–**5**, respectively, simulated in CH_2Cl_2 medium.

	1	**2**	**3**	**4**	**5**
HOMO	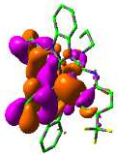	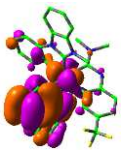	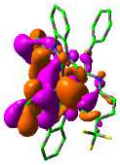	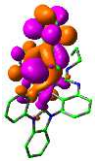	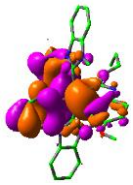
LUMO	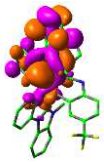		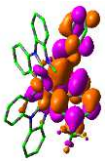	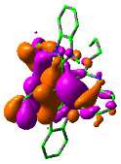	

Table 4 The triplet metal-to-ligand charge transfer ^{3}MLCT (%) in the T_1 state, the energy gaps between the S_1 and T_1 states $\Delta E_{S_1\text{-}T_1}$ (eV), the transition dipole moment in the $S_0 \rightarrow S_1$ transition μ_{s_1} (Debye) and the measured quantum yields Φ (%) for complexes **1**–**5** in CH_2Cl_2 medium

	^{3}MLCT	$\Delta E_{S_1\text{-}T_1}$	μ_{s_1}	Φ^a
1	21.33	0.208	0.111	1.3
2	16.62	0.763	0.040	
3	18.20	0.181	0.025	
4	22.40	0.180	0.100	
5	22.12	0.192	0.084	

[a] Ref. 19

Figures

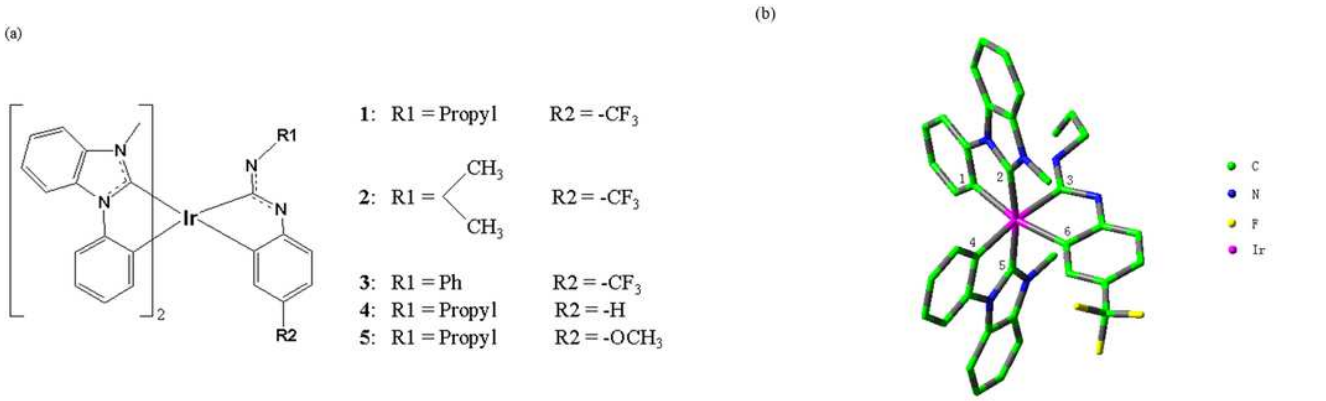

Figure 1

(a) Sketch map of the structures of Ir(III) complexes 1–5. (b) Representative optimized structure of 1 in the ground state at the PBE0 level (H atoms omitted).

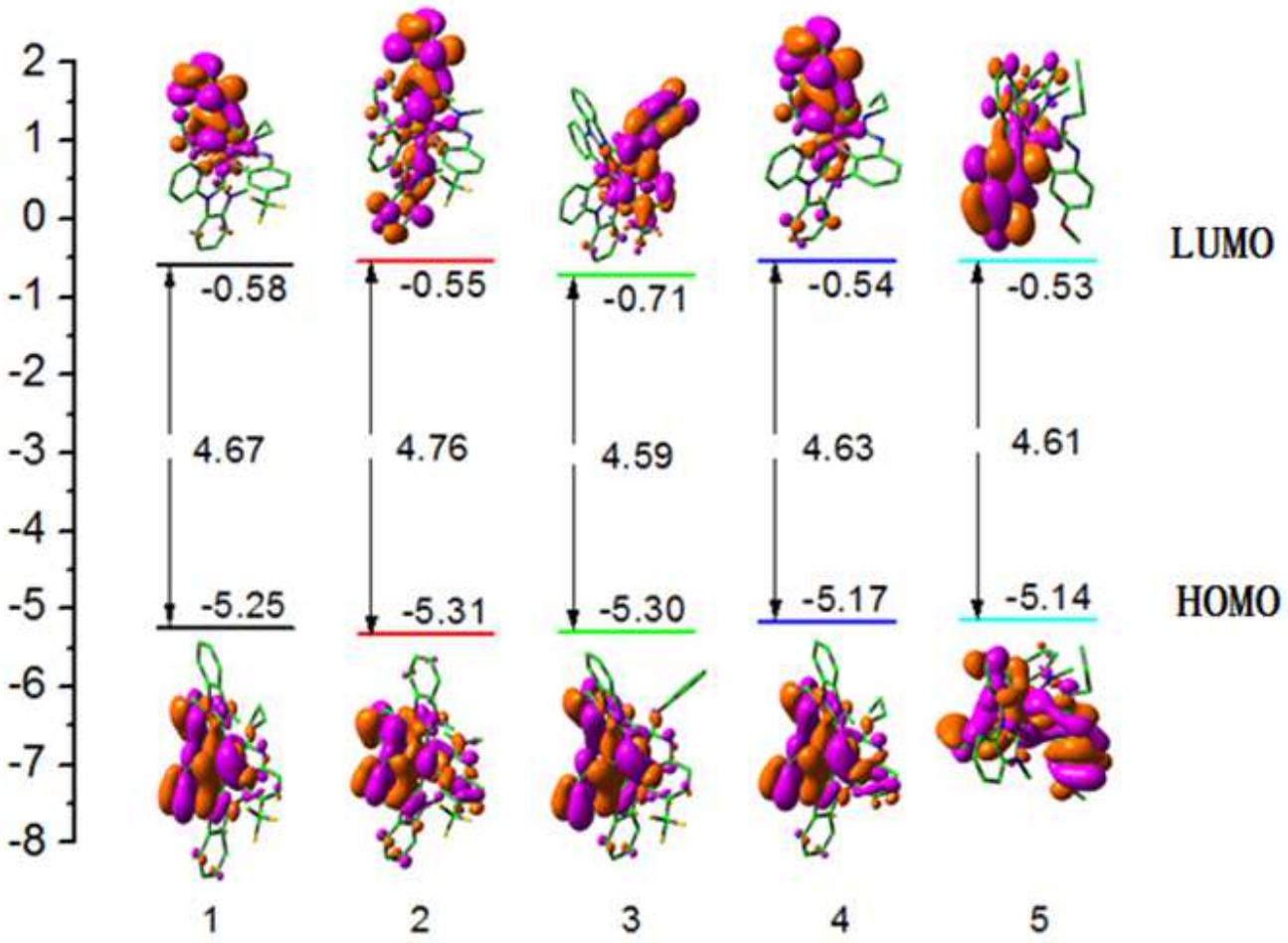

Figure 2

Contour plots of the HOMO and LUMO for complexes 1–5 in S0 state. The unit of data is eV.

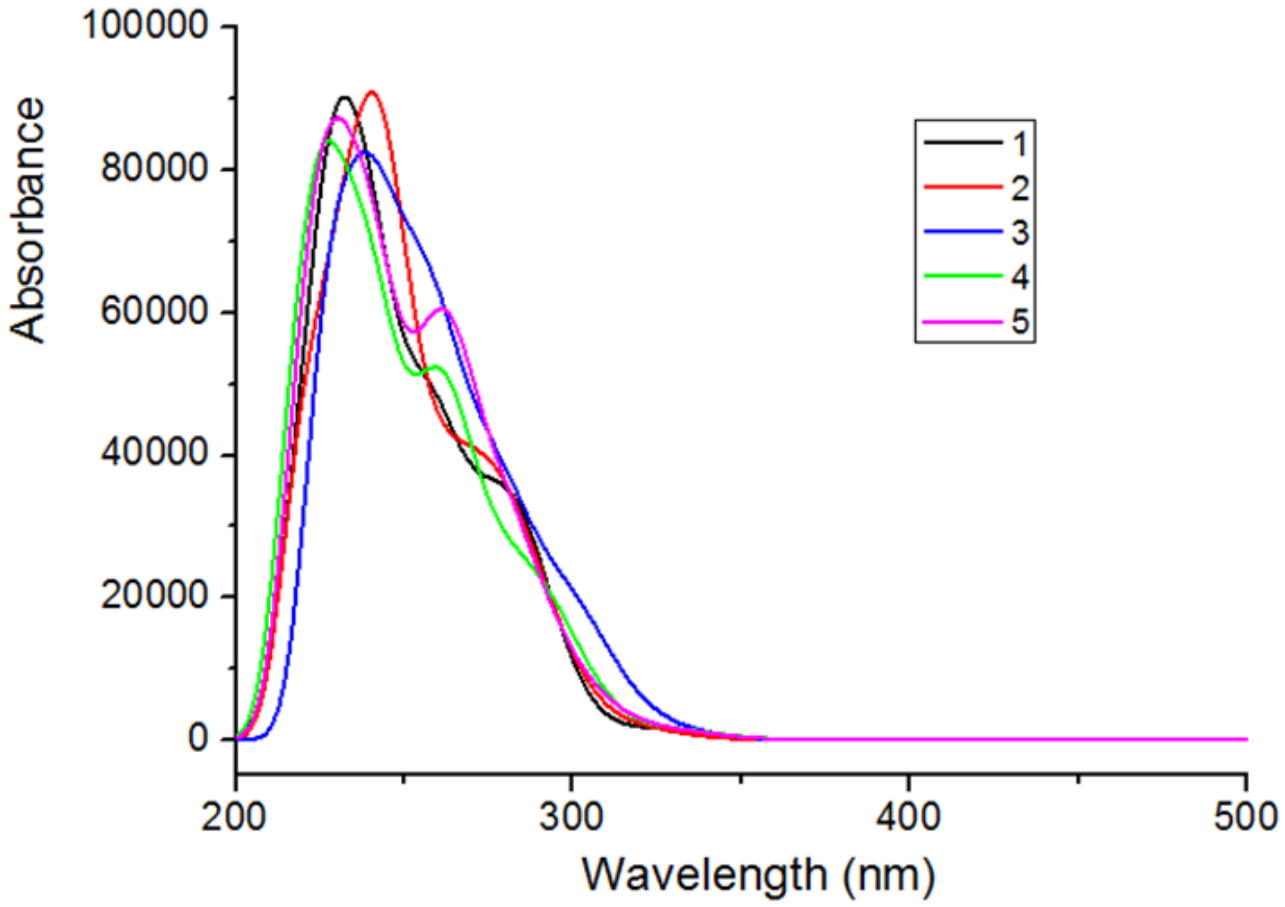

Figure 3

Simulated absorption spectra of complexes 1–5 in CH2Cl2 media.

Supplementary Files

This is a list of supplementary files associated with this preprint. Click to download.

- SupplementaryInformation.docx